![City, University of London logo]

City Research Online

City, University of London Institutional Repository

This is the accepted version of the paper.

This version of the publication may differ from the final published version.

Permanent repository link: https://openaccess.city.ac.uk/id/eprint/24785/

Link to published version: https://doi.org/10.1016/j.sna.2020.112214

Parallel structured fiber in-line multiple Fabry-Perot cavities for high temperature sensing

Hua Zhang[1], D. N. Wang[1,*], B. M. A. Rahman[2]

[1]*College of Optical and Electronic Technology, China Jiliang University, Hangzhou 310018, China*
[2] *School of Mathematics, Computer Science and Engineering, City University London, London, United Kingdom*

*E-mail: dnwang@cjlu.edu.cn

Abstract: We propose and demonstrate a parallel structured fiber in-line interferometric device consisting of two sets of periodic internal mirrors which forms Fabry-Perot cavities with different cavity lengths. The output of the device comprises two sets of overlapped fringe patterns, in which the main fringe peak is dominant and easy to identify. The cavity length of the internal mirror determines the spacing of the fringe peaks, which can be easily and flexibly controlled. The device is easy to operate or fabricated, simple in structure and exhibits high potential for high-temperature monitoring in harsh environments.

1. Introduction

Optical fiber sensor is considered as an attractive means for monitoring extreme environment, such as high temperature, due to its small size, light weight, flexible arrangement and free of electromagnetic interference [1-3]. Among various types of optical fiber sensors, interferometric sensors have shown high sensitivity. In particular, Fabry-Perot interferometers (FPIs) have compact size and a reflective structure, which is convenient for high temperature sensor monitoring in many cases [4-13]. In performing high temperature sensing by use of interferometric optical fiber sensors, typically a peak/dip wavelength in the output fringe pattern needs to be traced, as its shift corresponds to the temperature change. Such a tracing peak/dip wavelength has to be clearly identified.

Recently, a new technique has been developed which consists of multiple in-fiber reflection mirrors inscribed by femtosecond laser [14], thus forming many identical FP cavities cascaded along a single mode fiber (SMF) in an easy, flexible and reliable manner. There are many well-separated and dominant wavelength peaks in the output spectrum of the device, which helps improving the range and reliability of high temperature sensor monitoring. However, the output patterns of multiple cascaded FPIs have nearly equal intensity. In other words, it is hard to distinguish the tracing peak wavelength with its neighboring fringe in terms of intensity. This creates a difficulty in performing precision measurement especially for high temperature monitoring as a wide range of temperature change generates a large spectral shift, usually beyond the free spectral range of the interferometer.

Here, we present and demonstrate an in-fiber FPI in parallel structure which contains two sets of independent cascaded FP cavities. The output spectrum of the device is composed of two sets of overlapped FP fringe patterns, which results in the easily identified and tracked fringe peaks. The reliable system operation can then be achieved over a large measurement range. The interval between the fringe peaks depends on the two sets of FP cavity length, which can be easily controlled during the fabrication process. Moreover, due to the parallel structure,

such FPI system has a small device size. Thus, an accurate sensing position can also be determined. In addition, the device has also outstanding high temperature sustainability up to 1100ºC. The device is easy to operate and fabricated, simple in structure and has high potential for high-temperature monitoring in harsh environments.
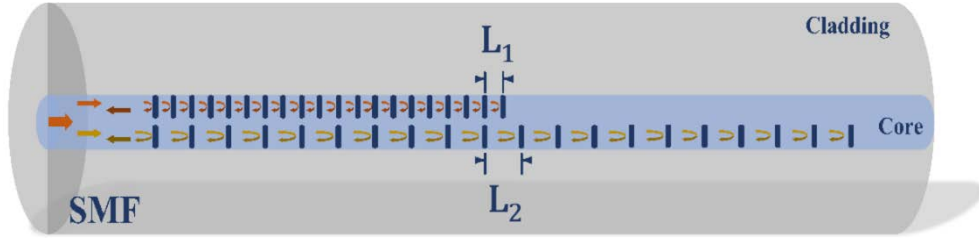
2. Principle

Fig. 1. The schematic diagram of the FPI device.

The schematic diagram of the presented device is illustrated in Fig. 1. By using the femtosecond laser micromachining technique, two sets of parallel cascaded internal mirrors with constant separation are engraved along the fiber core. The incident light beams propagating in the fiber core are sequentially reflected by the two sets of cascaded internal mirrors of different separations respectively, and the two groups of reflected beams are finally recombined in the fiber core to form the output spectrum of the FPI device. The end of the fiber is cut in an inclined surface to prevent any reflected light from returning to the fiber core. Since these mirrors are manufactured with the same femtosecond laser processing parameters, they can be considered to have similar reflectivity, and the reflectivity of each mirror is

$$R = \left[\frac{n_{mirror} - n_{core}}{n_{mirror} + n_{core}} \right]^2$$

(1)

where R is the reflectivity of the internal mirror, n_{mirror} and n_{core} are the refractive indices of the internal mirror and the fiber core respectively.

The propagation phase delays between the two sets of adjacent mirrors are given by

$$\varphi_1 = \frac{2\pi n_{core} L_1}{\lambda}$$

(2)

$$\varphi_2 = \frac{2\pi n_{core} L_2}{\lambda}$$

(3)

where L_1 and L_2 are the separations the two sets of mirrors, respectively and λ is the incident light wavelength.

For the parallel structured FPI consisting of two sets of cascaded mirrors inside the SMF, each set of internal mirrors has a constant separation. When the number of two sets of reflection mirrors reaches infinity, the total reflected light intensity can be approximately expressed as [14]

$$I = \frac{RE_0^2}{4(1+(1-\alpha)^2(1-R)^2 - 2(1-\alpha)(1-R)\cos 2\varphi_1)} + \frac{RE_0^2}{4(1+(1-\alpha)^2(1-R)^2 - 2(1-\alpha)(1-R)\cos 2\varphi_2)} \quad (4)$$

where E_0 is the electrical field of the incident light beam, R is the reflectivity of the internal mirror, α is the transmission loss factor at each internal reflection mirror.

3. Device Fabrication

The fabrication process by femtosecond laser for the presented in-fiber device is shown in Fig. 2(a). The femtosecond laser pulses used for device fabrication are produced from the regenerative amplified Ti: sapphire laser (Coherent Corp), with central wavelength of 800 nm, pulse energy of 800 µJ, pulse duration of 35 fs, repetition rate of 5 kHz. The core and cladding diameter of the SMF (SMF-28, Corning) used for device fabrication are 8.2 µm and 125 µm respectively, and the nominal effective RI is 1.4682 (at 1550 nm). The SMF to be inscribed is placed on a three dimensional micromachining platform (LASER µFAB, Newport Corp), which can achieve precise three-dimensional movement. The objective lens used for device fabrication is an oil-immersion objective lens of 100X magnification (NA = 1.25), which can eliminate the aberration introduced by the cylindrical state of SMF. For more precise processing, the moving speed of the focused beam is set to be slow, which is 2 µm / s.
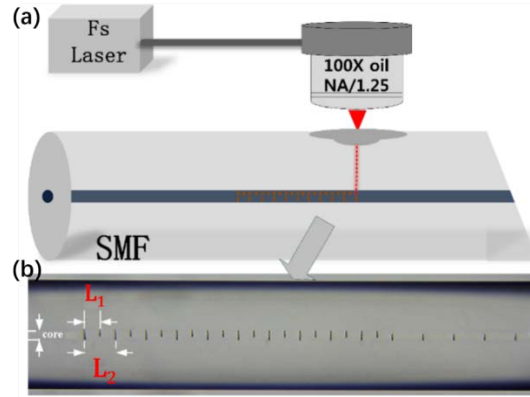

Fig. 2. (a) Femtosecond laser fabrication process of the parallel structured fiber in-line multiple FP cavities, (b) Microscope image of the device sample

As shown in Fig. 2(b), the cavity lengths of two independent parallel cascade FP cavities are 20 µm and 40 µm, respectively. The size of each mirror is basically the same, with height and thickness of 4 µm and 1 µm, respectively. The number of reflection mirrors for each cavity length is 20.

4. Experiments and Discussions

Based on Eq. (4), MATLAB software has been used to simulate the properties of parallel structured multiple FP cavities with different cavity lengths. Fig. 3 shows the results obtained for the output spectrum when the lengths of the two sets of FP cavities are 10 µm and 40 µm, 20 µm and 40 µm respectively (here the RI of the mirrors is assumed to be ~1.4846). It can be seen from Figs. 3(a) and 3(b) that, the interval of fringe peaks can be adjusted while maintaining the cavity length of one set of cascaded FP cavities, which enables a reliable system operation over a wide sensing range. It can be seen from the Fig. 3(c) that a relatively sharp peak can be

obtained when the cavity lengths of the two sets of FP cavity are 20 µm and 40 µm, which can be used to improve the fringe visibility.

The output spectrum of the FPI device sample with L_1 = 20µm, L_2 = 40 µm, are displayed in Fig. 4(a), where the simulated results are also shown for comparison. It can be observed from these figures that the experimental results agree very well with the simulated results.

It is noted that during the reflection mirror inscription that initially, the performance of dominant fringe peaks in terms of intensity and spectral width is gradually improved with the increase of the number of the reflection mirrors and then becomes stable after the number reaches a certain value.
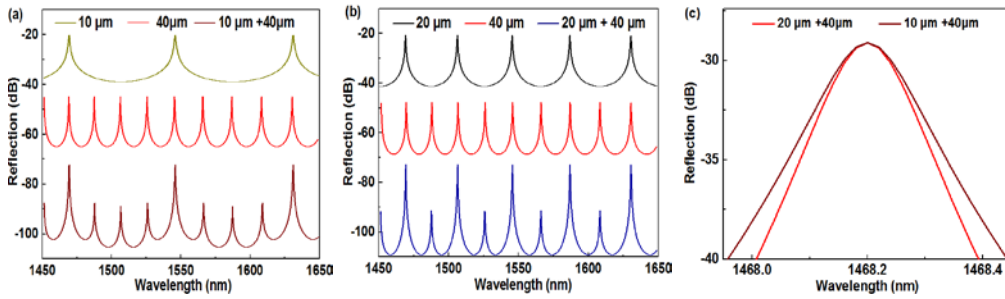

Fig. 3. (a) Simulated output spectrum of single set of cascaded FP cavities (L = 10 µm or 40 µm) and two sets of parallel structured cascaded FP cavities. (b) Simulated output spectrum of single set of cascaded FP cavities (L = 20 µm or 40 µm) and two parallel structured cascaded FP cavities. (c) Comparison of the spectral peaks for the parallel structured cascaded FP cavities with different separations.

Figure 4(b) show the Fourier transforms corresponding to the experimental output spectra of two parallel structured cascaded FPI devices shown in Fig. 4(a). In Fig. 4(b), the two main frequency peaks are located at 0.025 nm^{-1} and 0.05 nm^{-1}, respectively. The corresponding optical path differences (OPDs) are 58.125 µm and 116.25 µm, respectively, which are close to the calculated value of 58.728 µm and 117.456 µm, respectively.
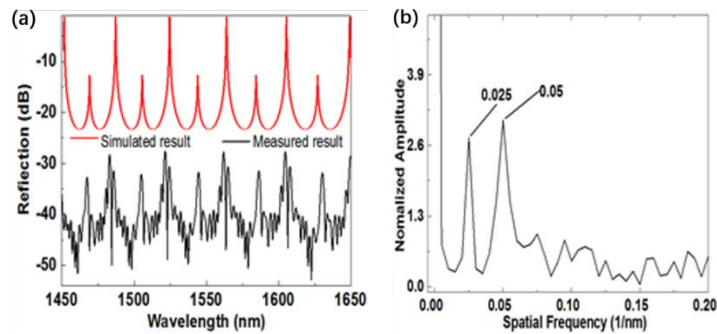

Fig. 4. The experimental and simulated output spectra of the device sample with (a) L_1 = 20µm, L_2 = 40 µm; frequency spectrum of the device sample with (b) L_1 = 20 µm, L_2 = 40 µm.
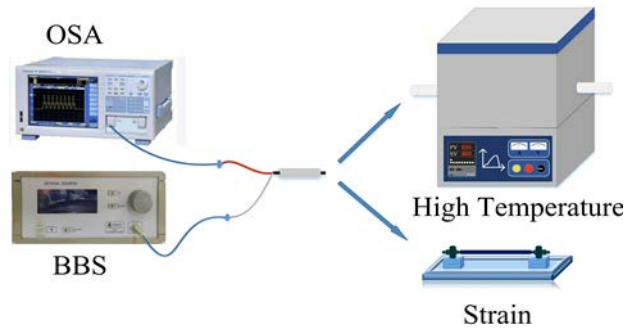
Fig. 5. Schematic diagram of Experiment system for (a) high temperature sensing test; (b) strain sensing test.

Figure 5 shows a schematic diagram of an experimental setup for the sensing tests. The incident light with a wavelength range of 1450 to 1650 nm from a broadband light source (BBS) (Connei) is introduced into the fiber FPI device via the circulator, and then the reflected output from the fiber device is directed to an optical spectrum analyzer (OSA) (YOKOGAWA 6390) with a resolution of 0.02 nm. The fiber device is mounted in a tube furnace during the high temperature test or on the fiber holder for a strain test. The device sample with cavity lengths of 20 μm and 40 μm respectively is used for the strain test and the for the high temperature test.

The FPI device sample is placed on two optical fiber mechanical clamps with a certain distance, and one of the clamps is mounted on a micrometer for applying axial strain on the device. As shown in Fig. 6(a), the peak of output spectrum moves toward the long wavelength as the strain increases. By linear fitting of the curve of peak wavelength versus strain, the strain sensitivity obtained is 1 pm/μɛ, with a linearity of 0.999, which is shown in Fig. 6(b).
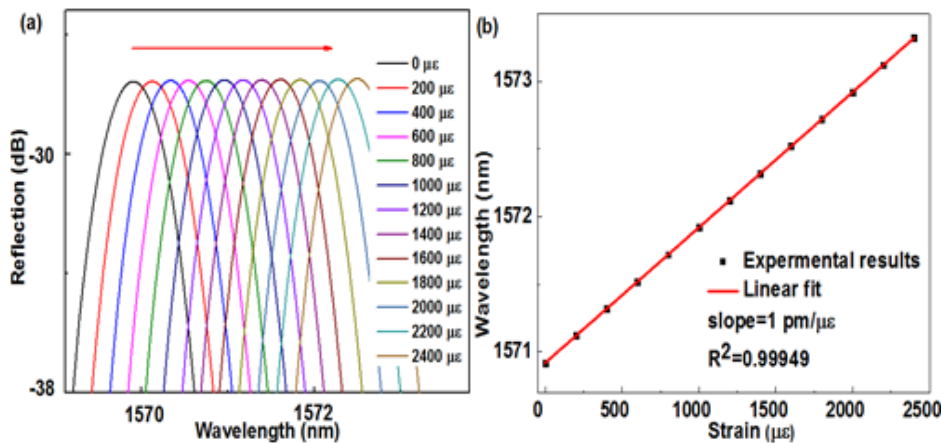

Fig. 6. Response of the device to strain. (a) Reflection spectra at different strains; (b) The peak wavelength shift versus strain.

As shown in Fig. 5, the high temperature sensing capability of the device was performed by placing the fiber device into the center of the tube resistance furnace with an accuracy of ±1°C (SANTE STG-40-17). Firstly, the optical fiber was annealed by heating the fiber device to 1100°C and maintaining at this temperature for 2 hours, before allowing it to cool down naturally to room temperature. During this period, the reflection spectrum of the device was monitored to ensure that no significant spectral change happened. This annealing process is to largely eliminate the residual stress in the fiber. After the annealing process and the temperature was gradually increased from room temperature to 100° C and then to 1100°C in a step of 100°C. After each step the temperature was maintained for ~30 minutes and the reflection spectrum data was recorded until the temperature was finally raised to 1100°C. The optical

fiber device was maintained at the temperature of 1100°C for 2 hours, and then cooled to room temperature in the same manner as that in the heating process.

Figure 7 shows the reflection spectra of the sensor device at different temperatures during the heating and the cooling processes, respectively. The reflection spectrum of the device after annealing is displayed in Fig. 7(a), where a blue shift of ~2 nm is found compared with that before the annealing process as shown in Fig. 4(a). However, the fringe pattern remains unchanged. Here, we use the position of the peak as the measured parameter, where the peak wavelength near 1572.5 nm is selected as the tracing wavelength. The spectral response with respect to high temperature is shown in Figs. 7(b) and 7(c), it can be observed that the spectra shift toward to the longer wavelength direction with the increase of temperature while to the shorter wavelength direction with the decrease of temperature. In the meantime, it can be observe that there is only a slight deviation (< 1nm) of the peak wavelength in the cooling process when compared to that in the heating process. The results obtained were also repeatable. The slope of the straight line obtained from data fitting shows the temperature sensitivity. According to the experimental results obtained, we divided the detection region into two parts, and a piecewise linear fitting was introduced as shown in Fig. 7(d). In the lower temperature region from 100 to 400°C, a linear fitting to the position of peak wavelength in the heating process is achieved and the wavelength shift slope obtained is 10.28 pm/°C, with R^2 value of 0.991. In the higher temperature range between 400 and 1100°C, a linear fitting to the position of peak wavelength in the heating process is achieved and the wavelength shift slope obtained is 16.91 pm/°C, with R^2 values of 0.99. The abrupt change of sensitivity slope at 400°C may be due to the residue stress introduced during the process of femtosecond laser inscription of reflection mirrors in the optical fiber.
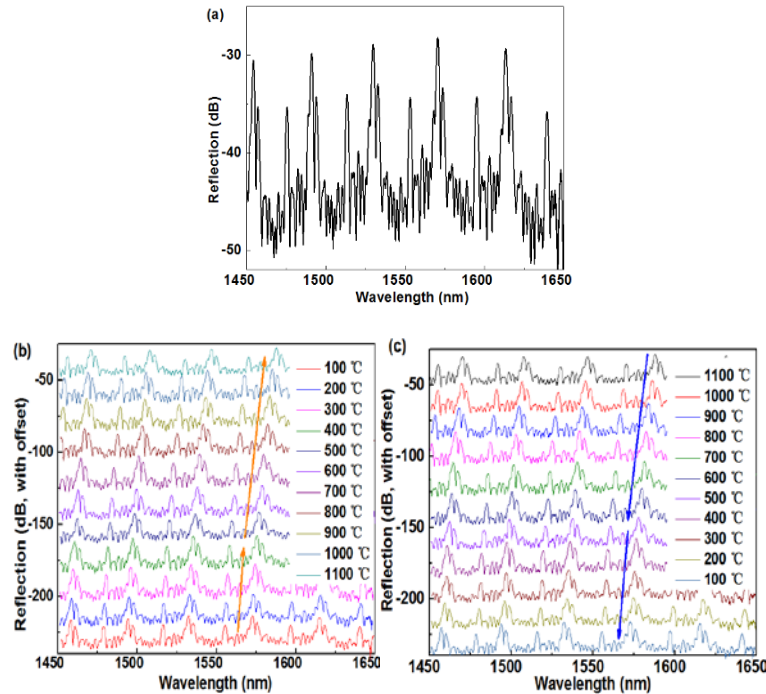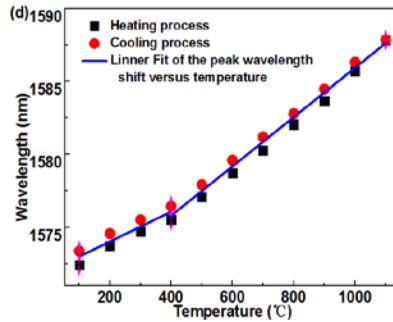
Fig. 7. (a) Reflection spectrum of the device after annealing. (b) Response of reflection spectrum of the device during the heating process. (c) Response of reflection spectrum of the device during the cooling processes. (d)The peak wavelength shift versus temperature.

5. Conclusion

In conclusion, we have demonstrated a parallel structured fiber in-line interferometric device which consists of two sets of multiple Fabry-Perot cavities with cavity length of 20 μm and 40 μm respectively. The output fringe pattern of the device is composed of two sets of overlapped FP fringe patterns, which results in the dominant fringe peak which is easy to be identified and tracked. By changing the combination of internal mirror separations of the parallel structured multiple FP cavities, the measurement range or the output fringe visibility of the device can be improved. The device developed is compact, robust and convenient in operation and has excellent high temperature sustainability, which makes it promising in extreme environment monitoring.

Acknowledgments

References

1. B. H. Lee, Y. H. Kim, K. S. Park, J. B. Eom, M. J. Kim, B. S. Rho, and H. Y. Choi, "Interferometric fiber optic sensors," Sensors. 12(3), 2467–2486 (2012).
2. Y. Wang, Y. Li, C. Liao, D. N. Wang, M. Yang, and P. Lu, "High-Temperature Sensing Using Miniaturized Fiber In-Line Mach–Zehnder Interferometer," IEEE Photon. Technol. Lett. 22, 39-41 (2010).
3. L. Xu, L. Jiang, S. Wang, B. Li, and Y. Lu, "High-temperature sensor based on an abrupt-taper Michelson interferometer in single-mode fiber", Appl. Opt. 52, 2038-2041 (2013).
4. X. Wan and H. F. Taylor, Intrinsic fiber Fabry-Perot temperature sensor with fiber Bragg grating mirrors, Opt. Lett., 27, 1388-1390 (2002)
5. Y. J. Rao, M. Deng, D. W. Duan, X. C. Yang, T. Zhu, and G. H. Cheng, Micro Fabry-Perot interferometers in silica fibers machined by femtosecond laser, Opt. Express, 15, 14123-14128 (2007)
6. T. Wei, Y. Han, H. L. Tsai, and H. Xiao, Miniaturized fiber inline Fabry-Perot interferometer fabricated with a femtosecond laser, Opt. Lett., 33, 536-538 (2008).
7. H. Y. Choi, K. S. Park, S. J. Park, Un-Chul Paek, B. H. Lee, and E. S. Choi, "Miniature fiber-optic high temperature sensor based on a hybrid structured Fabry–Perot interferometer," Opt. Lett. 33, 2455-2457 (2008).
8. P. Morrris, A. Hurrell, A. Shaw, E. Zhang, and P. Beard, A Fabry-Perot fiber-optic ultrasonic hydrophone for the simultaneous measurement of temperature and acoustic pressure, J. Acoust. Soc. Am., 125, 3611-3622 (2009).
9. T. Zhu, T. Ke Y. Rao, and K. S. Chiang, Fabry-Perot fiber tip for high temperature measurement, Opt. Commun., 283, 3683-3685 (2010).
10. W. Ding, Y. Jiang, R. Gao, and Y. Liu, High-temperature fiber-optic Fabry-Perot interferometeric sensors,

Review of Scientific Instrument, 86, 055001 (2013).

11. D. Lee, M. Yang, C. Huang, and J. Dai, Optical fiber high-temperature sensor based on dielectric films extrinsic Fabry-Perot cavity, IEEE Photon. Technol. Lett. 26, 2107-2110 (2014).

12. Jun Deng and D. N. Wang, Construction of cascaded Fabry-Perot interferometers by four in-fiber mirrors for high-temperature sensing, Opt. Lett., 44, 1289-1292 (2019).

13. Z. Zhang, J. He, B. Du, F. Zhang, K. Guo and Y. Wang, "Measurement of high pressure and high temperature using a dual cavity Fabry-Pérot interferometer created in cascade hollow-core fibers", Opt. Lett., 43, 6009-6012, (2018).

14. Jun Deng and D. N. Wang, Femtosecond laser inscribed multiple In-fiber reflection mirrors for high-temperature sensing, IEEE J. Lightwave Technol., 37, 4935-4939 (2019).